Monsoon-induced zonal asymmetries in moisture transport cause anomalous Pacific precipitation minus evaporation

P.M. Craig[1], D. Ferreira[2], and J. Methven[2]

[1]National Centre for Atmospheric Science, Department of Meteorology, University of Reading
[2]Department of Meteorology, University of Reading

Key Points:

- Atlantic and Pacific $P - E$ (precipitation minus evaporation) asymmetry is mainly due to atmospheric moisture transport and precipitation
- Moisture fluxes into the two polar ocean basins do not contribute significantly to the $P - E$ asymmetries between the Atlantic, Pacific and Indian Ocean basins
- Deviations from zonal mean zonal moisture flux associated with the summer monsoon flow across Southeast Asia dominate the $P - E$ asymmetry.

Corresponding author: Philip Craig, philip.craig@reading.ac.uk

Abstract

Basin-integrated precipitation minus evaporation ($P-E$) in the Pacific is near neutral while the Atlantic shows net evaporation. We link this $P-E$ asymmetry to atmospheric moisture fluxes across the boundaries of the ocean drainage basins. Adopting an objective approach based on a comparison between actual fluxes and a zonally averaged circulation, we show that the asymmetry is dominated by moisture fluxes associated with the monthly-mean flow in the Tropics rather than by differences in moisture fluxes into the Southern Ocean and Arctic catchments. In boreal summer, the eastward moisture flux, due to the Asian Summer Monsoon flow, opposes the zonal mean westward flux in the Trade Winds and results in more positive $P-E$ over the Pacific than both the Atlantic and Indian Oceans, even in the annual mean. Our results emphasize the role of atmospheric dynamics and moisture transport in the existence of the Atlantic/Pacific freshwater budget asymmetry.

1 Introduction

The contrast between Atlantic and Pacific sea surface salinity (SSS) is linked to the time-mean asymmetry in $P-E$ (precipitation minus evaporation) where the Atlantic $P-E \approx -0.5$ Sv ($1\ \text{Sv} \equiv 10^9$ kg s^{-1}) and the Pacific is near neutral. Craig et al. (2017) have shown the consistency of these estimates obtained from a range of atmospheric and oceanic analysis techniques. Both the SSS and $P-E$ asymmetries have been linked to the existence of a meridional overturning circulation (MOC) in the Atlantic and absence of a Pacific MOC (Broecker, 1991; Ferreira et al., 2010, 2018).

Previous studies have suggested that enhanced northward heat transport in the Atlantic by the Atlantic MOC (Trenberth & Caron, 2001) results in stronger Atlantic evaporation and the excess water vapour is transported in the Trade Winds across Central America to the Pacific causing weak net evaporation or net precipitation across the Pacific (Broecker, 1991). However, the Atlantic evaporation is only notably stronger in the subpolar region (Warren, 1983; Emile-Geay et al., 2003; Czaja, 2009; Wills & Schneider, 2015; Craig et al., 2017). There, sea surface temperatures are higher than in the Pacific (Warren, 1983; Manabe & Stouffer, 1988) and a greater fraction of the narrower basin is affected by advection of air off continents with low relative humidity (Schmitt et al., 1989) resulting in stronger area-averaged evaporation. However, the $P-E$ asymmetry exists at all latitudes (Craig et al., 2017). South of 30°N, the $P-E$ asymmetry is dominated by greater precipitation per unit area over the Pacific than the Atlantic. At the basin scale, evaporation rates per unit area across the Atlantic, Pacific and Indian Oceans are similar (Craig et al., 2017) and therefore precipitation differences dominate the $P-E$ asymmetry.

The vertical integral of the atmospheric moisture budget, implies that, in a sufficiently long time-average, the asymmetry in $P-E$ can only be balanced by differences in the convergence of atmospheric moisture flux into each ocean catchment. The drainage basins of the Atlantic, Pacific and Indian Oceans are defined by their continental divides, where they exist, and connected by segments across sea where necessary (see Figure 1, further details below).

The hypothesis that strong atmospheric moisture transport by the Trade Winds across Central America (Figure 2(b)) is the cause of the $P-E$ asymmetry between the Atlantic and Pacific appears often in the literature. Some authors specifically refer to the Isthmus of Panama (a very narrow strip of land) as the location of the Atlantic-to-Pacific moisture transport (Zaucker & Broecker, 1992;

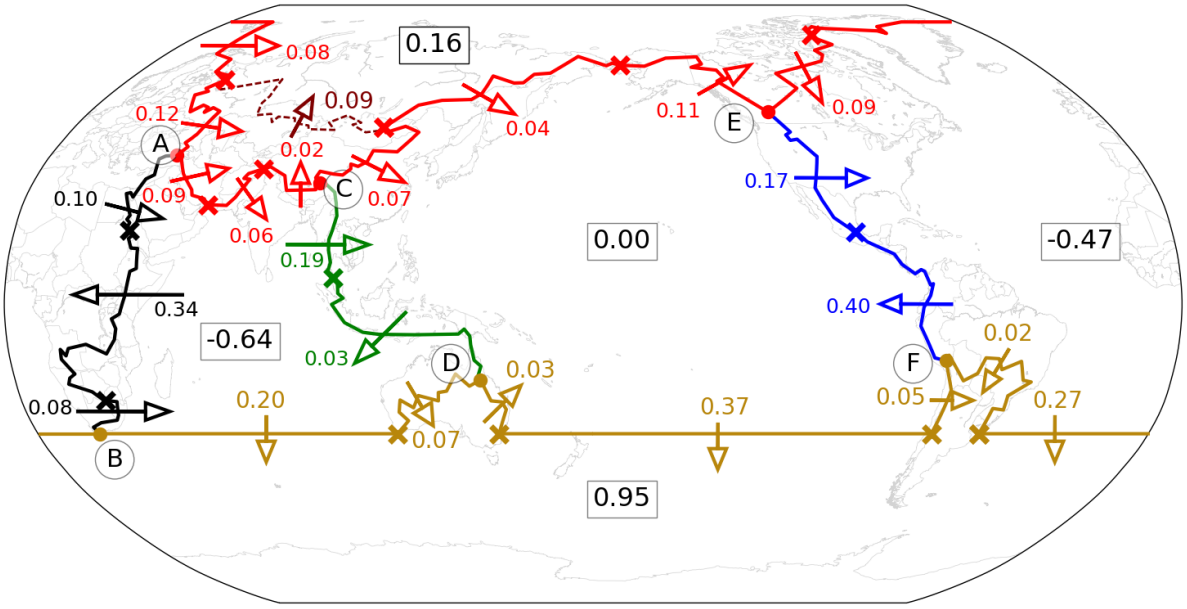

Figure 1. Vertically- and horizontally-integrated annual mean (1979-2014) ERA-Interim moisture fluxes normal to each catchment boundary (Q_{XY}) and basin-integrated precipitation minus evaporation ($\overline{P-E}$, boxes) calculated from Q_{XY} using equation (1). The large dots (labelled A, B, C, D, E and F) indicate the nodes of each sector of the Arctic (red) and Southern Ocean (gold) catchment boundaries where they meet the American (blue), African (black) and South-East Asian (green) catchment boundaries. The crosses show where the catchment boundaries are split into segments either based on the change in net direction of Q_{XY} or for geographical reasons. All units are Sverdrups (1 Sv $\equiv 10^9$ kg s^{-1}).

Lohmann, 2003; Leduc et al., 2007; Sinha et al., 2012) and other authors refer to Central America in general (Broecker, 1991; Richter & Xie, 2010; Schmittner et al., 2011; Wang et al., 2013). The emphasis on the moisture transport over Central America in explaining the $P-E$ asymmetry is based on two elements: 1) this flux is one of the strongest and is larger than the moisture flux over Africa at similar latitudes and 2) it is the shortest pathway from the Pacific to the Atlantic drainage basins.

Point 2 assumes that all Atlantic-to-Pacific atmospheric moisture transport across Central America is evaporated from the subtropical Atlantic and precipitated across the tropical Pacific (Leduc et al., 2007; Richter & Xie, 2010). This Eulerian understanding of the hydrological cycle ignores long-range atmospheric transport and potential remote sources of moisture and will be addressed in a separate paper.

Focusing on point 1, there is indeed strong moisture transport across Central America (0.29-0.72 Sv; Richter and Xie (2010)) as the lower orography relative to North and South America results in a reduced rain shadow effect while the moisture transport over Africa at similar latitudes is comparatively smaller (Broecker (1991); Figure 2(b)). However, it could be argued equally that the weakness of the moisture flux over Africa explains the divergent moisture transport over the Atlantic drainage basin. In other words, previous studies (cited above) highlighted the atmospheric moisture transport across Central America without providing a clear benchmark to objectively compare the relative contributions of the fluxes around the drainage basin to the asymmetry.

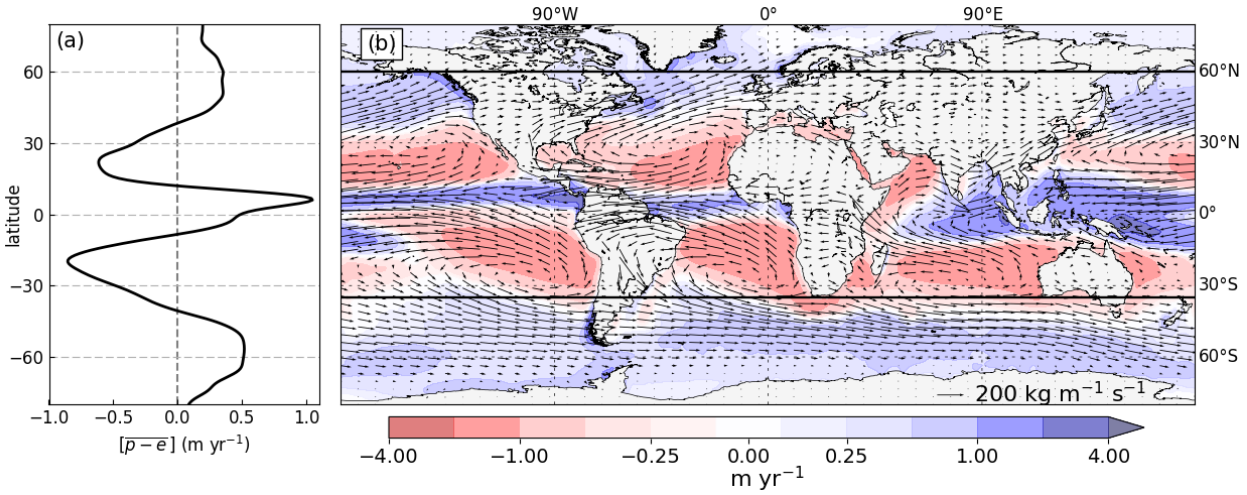

Figure 2. Annual mean (1979-2014) ERA-Interim $p - e$ (lowercase p and e represent local precipitation and evaporation rates) from vertically integrated moisture flux divergence: (a) zonal mean $[\overline{p-e}]$ from 80°S to 80°N and (b) global $\overline{p-e}$ (overbar denotes time mean) across the oceans (contours) and vertically-integrated moisture fluxes (arrows - see bottom right for scale). The black lines along 60°N and 35°S highlight the ocean basin latitude range referred to in the text.

Here, to study the Atlantic-Pacific $P - E$ asymmetry, we suggest that the zonally averaged atmospheric state is a useful reference state to compare moisture fluxes, especially those across the (quasi-) meridionally-orientated boundaries. One salient point is that the normal moisture fluxes, integrated along the meridionally-orientated boundaries, could not contribute to the $P - E$ asymmetries between basins if they were all equal to the zonal average zonal moisture flux. It is only deviations from the zonal average flux across these boundaries, or the fluxes into the Southern Ocean (SO) or Arctic basins, that could contribute to the $P - E$ asymmetries. Critically, the normal moisture flux across the American catchment boundary is approximately equal to the integral of the zonal mean zonal moisture flux across the same latitude range (Ferreira et al., 2018). It is therefore unlikely that the flux across the American catchment boundary contributes to the $P - E$ asymmetry between the Atlantic and Pacific as was suggested by previous studies.

Another salient feature arises from consideration of the zonally averaged $P - E$. The time-mean zonal-mean $P - E$ is negative in the subtropics and positive in the equatorial region and at high latitudes (summing up to zero when integrated globally) (Figure 2(a)). Therefore, over the latitude range of the Pacific basin, extending from approximately 35°S to 60°N, the zonal mean $P - E$ must be negative, as this range excludes the zone of net precipitation in the southern hemisphere high latitudes (Figure 2(b)). Atlantic and Pacific $P - E$ can be considered anomalous such that they deviate from the negative value obtained by integrating the zonal mean distribution over the area of the basin. The negative Atlantic $P - E$ is therefore much closer to the zonal averaged value, i.e. less anomalous, than the neutral Pacific.

In this paper, we will address the time mean $P - E$ asymmetry. To this end, we evaluate, in a quantitative and objective manner, the contributions of the moisture fluxes across catchment boundaries to the asymmetry using the zonally-averaged state as a reference point. Our analysis notably reveals that the moisture flux across Southeast Asia is the dominant factor in the $P - E$ asymmetry.

2 Data and Methods

Throughout this paper we use vertically-integrated horizontal water vapour fluxes from ERA-Interim reanalysis (Dee et al., 2011) over the period 1979 to 2014. The integral of moisture fluxes (Q_{XY}) normal to the catchment boundaries surrounding the ocean drainage basins (defined in the dataset Craig (2019)) are calculated using the formula:

$$Q_{XY} = \frac{1}{g}\int_X^Y \int_0^1 q\mathbf{V}\cdot\hat{\mathbf{n}}\frac{\partial p}{\partial \eta}\, d\eta\, dl \tag{1}$$

where dl denotes the line element along boundary XY, $\hat{\mathbf{n}}$ is its unit normal vector, $\mathbf{V}$ is the horizontal wind vector, q is specific humidity, η is the vertical coordinate of the ERA-Interim data and p is pressure. These are linked precisely to $P-E$ through the divergence theorem (see Supporting Information; SI). Note that Craig et al. (2017) present $E-P-R$ including the runoff, R, estimated with Dai and Trenberth (2002)'s river discharge dataset. Here, $\overline{P-E}$ for an ocean drainage basin incorporates R as it is approximately equal to net precipitation over land assuming that storage fluxes are relatively small in the monthly average. See the SI for more details on the data and methods.

3 Annual Mean Moisture Fluxes and Basin-Integrated $P-E$

The annual average $P-E$ for the five ocean basins and the integral fluxes across the various segments of the boundaries surrounding the basin catchments are shown in Figure 1. General features are that moisture fluxes are mainly crossing the boundaries eastwards in the extratropics, and also polewards across 35°S into the SO basin. In the tropics transport crosses the boundaries westwards in the Trade Winds, with the notable exception of Southeast Asia (boundary CD) where the annual average flux is in the opposite direction.

Across the American boundary (EF) westward atmospheric moisture transport in the tropics is partially offset by eastward transport in the mid-latitudes. In contrast, across the northern section of the Southeast Asian catchment boundary (CD) there is an eastward moisture flux associated with the annual mean flow across India and the Bay of Bengal. The $\overline{P-E}$ values calculated from Q_{XY} surrounding the Atlantic, Indian and Pacific Oceans are consistent with the various estimates compared in Craig et al. (2017). Other authors have presented maps similar to Figure 1 (Rodriguez et al., 2011; Levang & Schmitt, 2015; Singh et al., 2016) but in some estimates Q_{CD} is weaker than, or of opposing sign to, Figure 1. This appears to be a consequence of coarse resolution and problems with representing the Walker Circulation (Schiemann et al., 2014) and winds over the equatorial Indian Ocean (Goswami & Sengupta, 2003). Some studies present a CD boundary wildly different from Figure 2 which results in a weaker Q_{CD} but does not substantially change the $\overline{P-E}$ asymmetries. These estimates are discussed in more detail in the SI.

A common interpretation of Figure 1 is that the westward Atlantic-to-Pacific transport across the southern end of the American boundary (0.40 Sv) dominates the $\overline{P-E}$ asymmetry as it is the largest flux entering the Pacific (Broecker, 1991; Zaucker & Broecker, 1992; Richter & Xie, 2010). However, this ignores the net eastward Indian-to-Pacific transport, Q_{CD}, across South-East Asia (0.16 Sv). Atmospheric moisture converges into the Pacific drainage basin across both its western (CD) and eastern (EF) boundaries while the net transport is westward across both the western (EF) and eastern (AB) boundaries of the Atlantic basin. There is also net export of atmospheric moisture across all four catchment boundaries of the Indian drainage basin (resulting in strong net moisture flux divergence)

and therefore the Indian Ocean acts as a source of moisture for both the Atlantic and Pacific Oceans (Stohl & James, 2005; Craig, 2018).

Sub-monthly moisture fluxes across the Arctic and SO boundaries are always poleward (with the exception of the River Plate drainage basin) reflecting the net poleward moisture transport in mid-latitude weather systems (Pfahl et al., 2015; Dey & Döös, 2019). Sub-monthly poleward fluxes across 35°S to the So are similar per unit length along each sector (Table S2) and therefore cannot account for the Atlantic/Pacific $\overline{P-E}$ asymmetry. Similar conclusions can be drawn for the sub-monthly fluxes into the Arctic; fluxes associated with the monthly-mean flow are discussed in Section 5.2.

The sub-monthly fluxes across the boundaries between the Atlantic, Pacific and Indian Oceans are very small compared to those associated with the monthly-mean flow (Figure S1). The mean flow results in net precipitation across the Pacific but sub-monthly processes result in net evaporation with the strongest Q'_n across 35°S. The $\overline{P-E}$ asymmetry is therefore dominated by the monthly-mean flow across the African, South-East Asian and American boundaries.

4 Seasonal Cycle in Moisture Fluxes and $P-E$

The Atlantic/Pacific $\overline{P-E}$ asymmetry is greatest in JJA (>1 Sv) when the net Southeast Asian flux Q_{CD} is eastward (0.59 Sv), associated with the Asian Summer Monsoon, and the westward net flux across the Americas, Q_{EF}, peaks (0.38 Sv) associated with the maximum strength of the Caribbean low-level jet (LLJ) (Wang et al., 2013). Both converge moisture into the Pacific basin, resulting in $\overline{P-E}=0.55$ Sv in JJA (Figure 3(c)). The JJA peak in Q_{EF} coincides with minimum African flux, Q_{AB}, (0.08 Sv) as the Somali LLJ diverts moisture away from Africa (Riddle & Cook, 2008) thus contributing to peak Atlantic net evaporation (-0.63 Sv, Figure 3(c)). The moisture storage term, $\partial(TCWV)/\partial t$ (Equation 1 in SI), is more important in the seasonal cycle than in annual climatologies (Berrisford et al., 2011; Trenberth et al., 2011) but is only significant in the Pacific in JJA where it exceeds the divergence of Q_n by 0.01 Sv (Table S1). Atlantic and Pacific $\partial(TCWV)/\partial t$ are of the same sign in JJA so the magnitude of the $\overline{P-E}$ asymmetry is only slightly affected by the storage of moisture in the seasonal cycle.

The seasonal cycle of the Atlantic/Pacific $\overline{P-E}$ asymmetry is therefore strongly influenced by the meteorology of the Indian Ocean and the dynamics of the Asian Monsoon (Stohl & James, 2005; Baker et al., 2015; Craig, 2018; Volonté et al., 2019) as the direction of Q_{CD} only changes with season. The annual mean moisture flux field (Figure 2(b)) over the Indian Ocean, Maritime Continent and North-West Pacific is dominated by JJA, as is Pacific $\overline{P-E}$ since it is negative during the rest of the year, but strongly positive in JJA, enabling the Pacific basin to be neutral in the annual mean (Figure 3). Emile-Geay et al. (2003) first suggested a role for the Asian Monsoon in the $\overline{P-E}$ asymmetry but only for the subpolar regions, while Craig et al. (2017) showed that the $\overline{P-E}$ asymmetry is dominated by stronger Pacific precipitation per unit area south of 30°N.

5 Understanding the $P-E$ Asymmetry by a Process of Elimination

The evidence has now been presented which will enable the deduction that the atmospheric moisture flux across Southeast Asia (the catchment boundary CD) is the dominant reason for the asymmetry in $\overline{P-E}$ integrated over the Pacific compared with the Atlantic and Indian Ocean basins. The argument

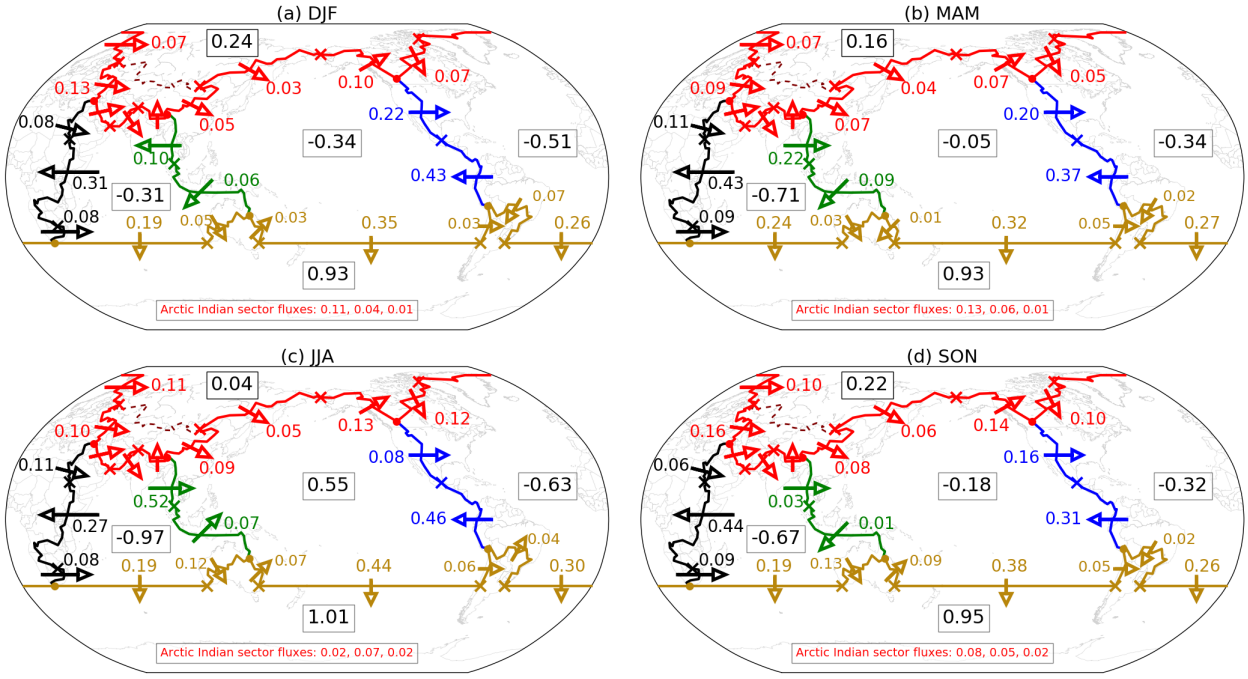

Figure 3. Climatological seasonal means (1979-2014) of $\overline{P-E}$ (boxes) and vertically- and horizontally-integrated moisture fluxes normal to each catchment boundary (arrows) split into sections based on geographic locations or change in the net direction of annual mean Q_n. All values are in Sverdrups (1 Sv $\equiv 10^9$ kg s^{-1}) and rounded to two significant figures.

detailed below follows a process of elimination where the influence of moisture exchange with the Arctic and SO catchments are discounted and so are sub-monthly moisture fluxes in the Tropics. The final argument regards the moisture flux associated with the monthly-mean flow across the three boundaries AB, CD and EF.

5.1 Poleward flux across 35°S into the Southern Ocean catchment

The net moisture flux poleward across 35°S is strongest in the Pacific sector (0.37 Sv) and weakest in the Indian sector (0.20 Sv) (Figure 1). However, the relative widths of the basins at 35°S (the Pacific is wider than the Atlantic and Indian Oceans by a factor of 1.8 and 1.5 respectively) dominates this variation. Sub-monthly fluxes are approximately equal when scaled by unit length along the boundary and therefore do not make a significant contribution to asymmetries in $\overline{P-E}$ (Table S2).

However, Q_n^m is an order of magnitude larger in the Atlantic than in the Pacific. Possible reasons for this are:

1. a greater fraction of the Atlantic is occupied by southward $\overline{q}\,\overline{v}$ (Figure S2) while in the Pacific the subtropical high is confined to the east of the basin (see Figure 2(b)).
2. the easterly trade winds are deflected to the south by the Andes resulting in strong southward $\overline{q}\,\overline{v}$ over South America and a region off the east coast of Brazil.
3. the South Pacific Convergence Zone may weaken $\overline{q}\,\overline{v}$ in the South Pacific as it causes anomalous moisture flux convergence into a region which has no analogue in the Atlantic (Figure S2).

Nevertheless, this Q_n^m asymmetry is small compared with the difference in $\overline{P-E}$ between the Pacific and Atlantic.

5.2 Moisture exchange with Arctic

Atmospheric moisture imported into the Pacific drainage basin across Asia between the Himalayas and Bering Strait (0.11 Sv, Figure 1) is balanced by moisture exported across Canada and Alaska in the mid-latitude westerlies. Therefore, net Q_{DF} across the Pacfic sector of the Arctic catchment boundary is approximately zero. Moisture imported across Canada into the Atlantic basin (0.09 Sv) is almost balanced by atmospheric moisture export into the Arctic (0.08 Sv) at the end of the North Atlantic storm track. However, net moisture flux across the Atlantic sector of the Arctic catchment boundary is dominated by zonal transport of 0.12 Sv across Europe into the Central Asian endorheic basin (i.e. isolated from the global ocean) where $\overline{P-E} \approx 0$ Sv (Stohl & James, 2005). This results in a net export of atmospheric moisture from the Atlantic basin into the Arctic basin which contributes 0.11 Sv to the net negative $\overline{P-E}$ of the Atlantic.

This asymmetry is related to the shape of the Arctic catchment boundary (Figure 1). The Atlantic sector extends further south at its eastern end (Turkey) than the Pacific sector (southern Canada) so zonal moisture fluxes act to export moisture from the Atlantic into the Arctic across Eastern Europe (Figure 2). This accounts for the majority of the net positive $\overline{P-E}$ of the Arctic basin. The remainder of moisture flux convergence into the Arctic basin comes across the neighbouring boundary over the Middle East from the Indian Ocean basin.

As introduced in Section 3, the sub-monthly flux $Q_n^{'}$ across boundaries BD, DF and FB is directed everywhere into the Arctic, and does not contribute significantly to the $\overline{P-E}$ asymmetry. However, Q_n^m from the Atlantic into the Arctic does contribute 0.11 Sv to the asymmetry (making $\overline{P-E}$ more negative for the Atlantic) since the net flux from the Pacific into the Arctic is approximately zero.

5.3 Anomalous Moisture Flux Across the Meridional Boundaries

As discussed in section 1, the moisture fluxes across the "meridional" boundaries AB, DC and EF (Figure 1) can only contribute substantially to the $\overline{P-E}$ asymmetry if they differ, when integrated, from the zonal mean flux across the same latitude range - otherwise just as much moisture would leave as entered each catchment across these boundaries. Figure 4 compares profiles of American, African and South-East Asian Q_n to the zonal mean zonal moisture flux, $[\overline{qu}]$, as well as the corresponding integrals over the segments AB, CD, and EF.

The integral flux across the American boundary, Q_{EF}, almost matches the integral of $[\overline{qu}]$ across the same range of latitudes with a difference of only 0.01 Sv (Figure 4(a)). The most significant deviation of Q_n from $[\overline{qu}]$ occurs at 11°N above Lake Nicaragua in the Papagayo jet (Clarke, 1988) with a peak at 265 kg m^{-1} s^{-1}. The other peaks along Central America are at 17°N through the Chivela Pass from the Tehuantepec jet and at 9°N from the Panama jet (Steenburgh et al., 1998). Above Panama, Q_{EF} is less than $[\overline{qu}]$ so, contrary to previous literature (Zaucker & Broecker, 1992; Lohmann, 2003; Leduc et al., 2007; Sinha et al., 2012), moisture flux across Panama cannot be the dominant aspect of the $\overline{P-E}$ asymmetry.

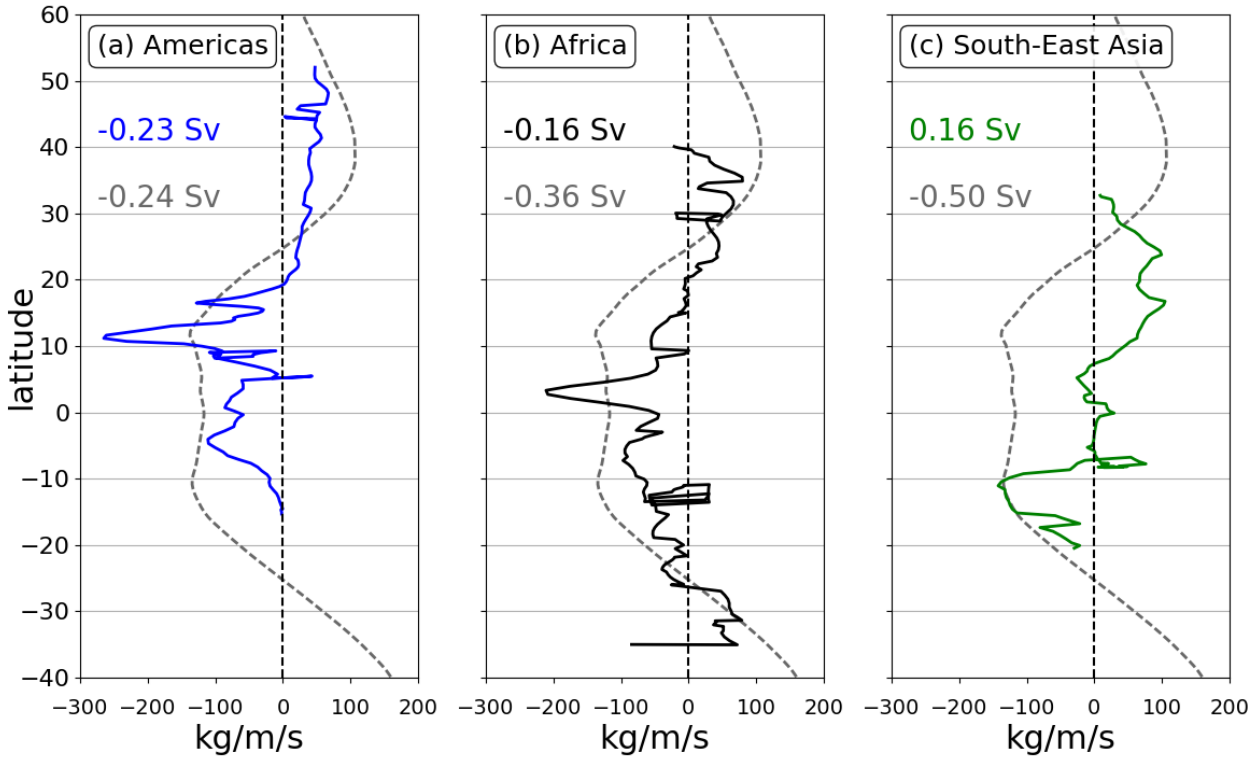

Figure 4. Comparison between the zonal mean zonal moisture flux ($[\overline{qu}]$, dashed lines) and the profile of the moisture flux normal to the (a) American, (b) African and (c) South-East Asian catchment boundaries (Q_n, solid lines). The coloured numbers show the integrated fluxes, Q_{EF}, Q_{AB} and Q_{CD}, for the respective catchment boundaries and the grey numbers show the integral of $[\overline{qu}]$ between the latitude limits of each catchment boundary.

The profile of African Q_n also bears some similarity to $[\overline{qu}]$ with a peak at 3°N (210 kg m^{-1} s^{-1}) in northern Kenya from the Turkana LLJ between the Ethiopian Highlands and East African Highlands (Nicholson, 2016). The integral flux Q_{AB} has the same sign as the integral of $[\overline{qu}]$ between the corresponding latitudes but is 0.20 Sv weaker (Figure 4(b)).

The profile of Southeast Asian flux paints a very different picture to its American and African counterparts (Figure 4(c)). Deviations from $[\overline{qu}]$ along the Southeast Asian catchment boundary are far larger than those along the American and African catchment boundaries. Much of Q_n is of opposite sign to $[\overline{qu}]$, particularly across Thailand. The two only match between 10°S and 15°S above the Torres Strait between Australia and Papua New Guinea. The integral Q_{CD} is therefore of opposite sign to the corresponding integral of $[\overline{qu}]$, giving a net anomalous moisture export of 0.66 Sv (difference between integral of $[\overline{qu}]$ and Q_{CD}) from the Indian Ocean drainage basin to the Pacific.

To demonstrate the role of deviations of the integral moisture fluxes Q_{AB}, Q_{CD} and Q_{EF} from $[\overline{qu}]$ in setting the $\overline{P-E}$ asymmetry, we conduct a thought experiment by considering a zonally symmetric atmospheric circulation where moisture fluxes across the African, American and Southeast Asian boundaries match the corresponding integrals of $[\overline{qu}]$ across their respective latitude ranges (Figure 5). The implied net $\overline{P-E}$ over each ocean basin is then computed from the modified $\tilde{Q}_{AB}$, $\tilde{Q}_{CD}$ and $\tilde{Q}_{EF}$ keeping fluxes across the Arctic and SO boundaries unchanged.

If the fluxes across AB, CD and EF each matched $[\overline{qu}]$ (Figure 5(a)), $\overline{P-E}$ would be negative in the Pacific, Atlantic and Indian Ocean basins as expected (see section 1). Furthermore, the three ocean basins would have similar $\overline{P-E}$ per unit area (Table S3). This also reinforces that moisture fluxes to the Arctic and SO play minor roles in the $\overline{P-E}$ asymmetry. When the flux across Africa is reverted to its "real world" value less atmospheric moisture flux is leaving the Indian Ocean basin and enters the Atlantic basin, so Indian $\overline{P-E}$ becomes approximately neutral and Atlantic net evaporation is stronger, matching the "real world" value (Figure 5(b)).

There is very little impact on Pacific and Atlantic $\overline{P-E}$ when the flux across the Americas Q_{EF} is reverted to its "real world" value since it is almost the same as the integral of $[\overline{qu}]$ (Figure 4(a)). Reverting the flux across Southeast Asia to its "real world" value, Q_{CD}, reverses the sign relative to the zonal-mean flux (Figure 5(c)). The Indian Ocean now becomes strongly evaporative and Pacific $\overline{P-E}$ becomes neutral as seen in Figure 1. In summary, the thought experiment shows that deviations from $[\overline{qu}]$ along the South-East Asian catchment boundary dominate the $\overline{P-E}$ asymmetry between the Atlantic and Pacific Oceans, and as well as between the Indian and Pacific Oceans.

6 Conclusions

Through a process of elimination, it has been deduced that the atmospheric moisture flux across Southeast Asia, especially during the Asian Summer Monsoon, is the dominant factor establishing the $\overline{P-E}$ asymmetry between the Pacific, Atlantic and Indian Oceans. The steps in the argument eliminating other factors are:

1. Moisture fluxes into the SO basin are dominated by sub-monthly fluxes which are everywhere poleward with similar Q'_n per unit length along each sector of 35°S (Table S2). Therefore, fluxes across the SO boundary do not contribute to the $\overline{P-E}$ asymmetry.
2. Fluxes associated with the monthly-mean flow are greater across some segments of the Arctic boundary compared with the poleward flux from the sub-monthly fluxes. However, the net flux between the Pacific and Arctic is almost zero while there is a net flux into the Arctic from the Atlantic basin of 0.11 Sv. This contributes almost one quarter of the $\overline{P-E}$ asymmetry.
3. Sub-monthly fluxes (Q'_n) across the American, African and Southeast Asian boundaries (Figure S1) are very small compared to the flux by the monthly-mean flow.
4. Integral moisture fluxes across the African, Southeast Asian and American boundaries, Q_{AB}, Q_{CD} and Q_{EF}, only contribute to ocean basin asymmetry in $\overline{P-E}$ such that they deviate from the zonal mean zonal moisture flux ($[\overline{qu}]$) integrated over the same latitude range. The net flux across the Americas, Q_{EF}, approximately equals the integral of $[\overline{qu}]$ and therefore does not contribute to the $\overline{P-E}$ asymmetry (Figures 4 and 5, Table S3).

The deviation of the flux across Southeast Asia, Q_{CD}, from $[\overline{qu}]$ dominates the annual mean state of the asymmetry. The net eastward moisture flux of 0.59 Sv during the Asian Summer Monsoon generates a large deviation from the westward zonal mean flux, even in the annual average. This causes annual mean Pacific $\overline{P-E}$ to be approximately neutral rather than the net evaporation ($\overline{P-E} \approx -0.66$ Sv) calculated using $[\overline{qu}]$ across the latitude range of boundary CD (Figure 4).

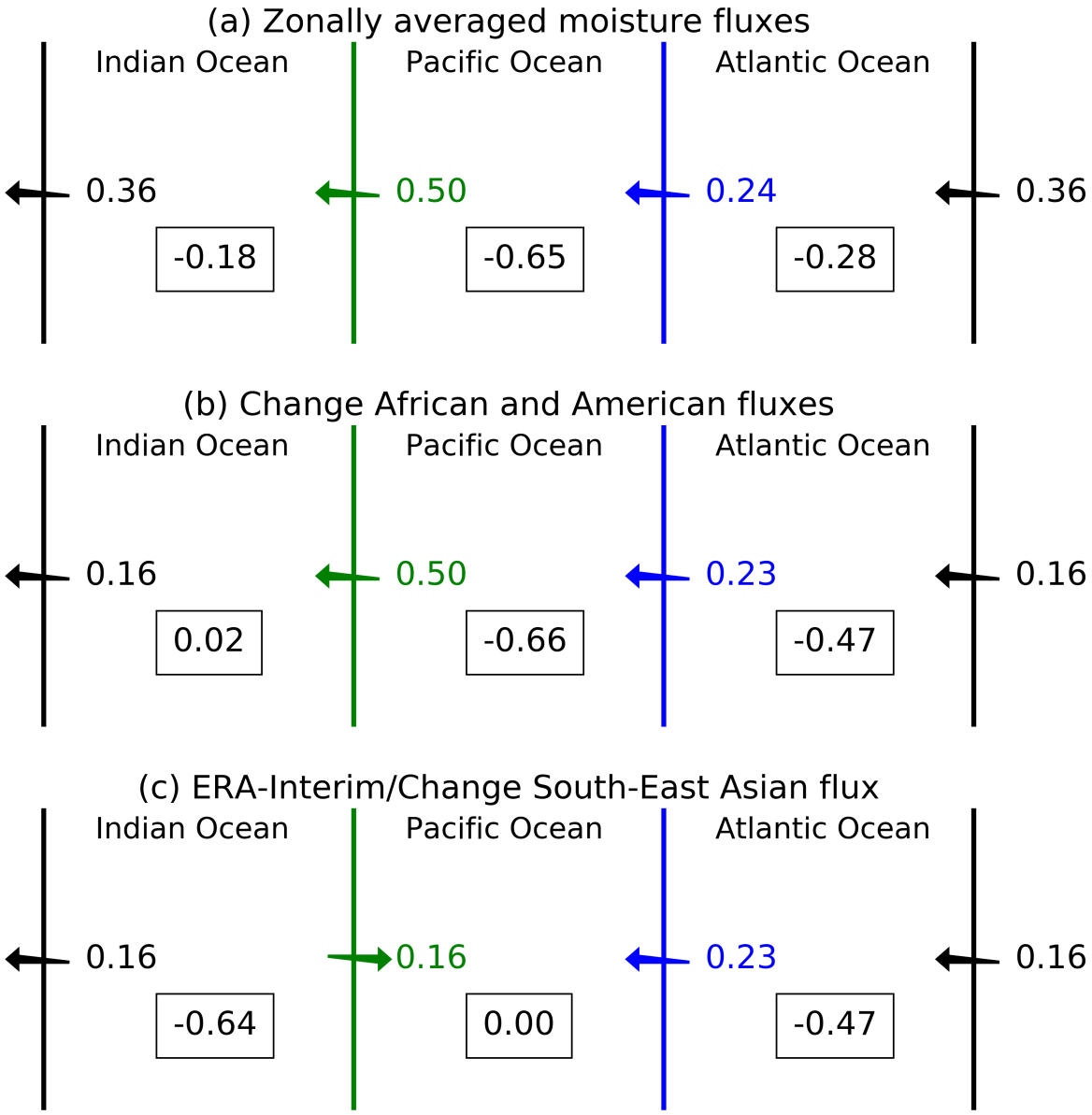

Figure 5. A thought experimentillustrating the influence of integral moisture fluxes across the catchment boundaries between the Atlantic, Indian and Pacific Oceans. (a) Basin-integrated $P - E$ (values in boxes) in the hypothetical situation that the normal fluxes across boundaries AB, CD and EF were equal to zonal mean zonal moisture fluxes. (b) Reverting the fluxes across the African and American catchment boundaries to the observed values Q_{AB} and Q_{EF} and consequences for $P - E$. (c) Reverting the flux across the Southeast Asian boundary to the observed value, Q_{CD}, recovering the ERA-Interim "real world" estimates in all catchments. Note that moisture transports across the Arctic and SO catchments remain unchanged. Fluxes and $\overline{P - E}$ are given in Sv.

The seasonal cycles of Q_{XY} and $\overline{P - E}$ show that Southeast Asian Q_{CD} changes direction, and African Q_{AB} weakens, during the Asian Summer Monsoon in JJA. This results in a strong excess of precipitation over evaporation across the Pacific, a peak in Indian Ocean net evaporation (Figure 3c) and also a reduction of moisture flux into the Atlantic across Africa. The role of the Asian Monsoon has been identified as an important factor previously (Emile-Geay et al., 2003; Czaja, 2009; Ferreira et

al., 2018) but we present the first quantification of its impact and argue that it affects the basin scale asymmetry, rather than just the subpolar asymmetry, between the Atlantic and Pacific Oceans.

Acknowledgments

The lead author received PhD studentship funding from the Natural Environment Research Council as part of the SCENARIO Doctoral Training Partnership (NE/L002566/1). The dataset defining the ocean catchment boundaries is available from the University of Reading Research Data Archive: `http://dx.doi.org/10.17864/1947.195`. The ERA-Interim dataset was made available by ECMWF.

References

Baker, A., Sodemann, H., Baldini, J., Breitenbach, S., Johnson, K., van Hunen, J., & Pingzhong, Z. (2015). Seasonality of westerly moisture transport in the East Asian summer monsoon and its implications for interpreting precipitation δ^{18}O. *Journal of Geophysical Research: Atmospheres*, *120*, 5850-5862.

Berrisford, P., Kållberg, P., Kobayashi, S., Dee, D., Uppala, S., Simmons, A., ... Sato, H. (2011). Atmospheric conservation properties in ERA-Interim. *Quarterly Journal of the Royal Meteorological Society*, *137*, 1381-1399.

Broecker, W. (1991). The Great Ocean Conveyor. *Oceanography*, *4*, 79-89.

Clarke, A. (1988). Inertial wind path and sea surface temperature patterns near the Gulf of Tehuantepec and the Gulf of Papagayo. *Journal of Geophysical Research: Oceans*, *93*, 15491-15501.

Craig, P. (2018). *The Atlantic/Pacific Atmospheric Moisture Budget Asymmetry: The Role of Atmospheric Moisture Transport* (Unpublished doctoral dissertation). University of Reading.

Craig, P. (2019). *Catchment Boundaries of Ocean Drainage Basins.* University of Reading. Dataset: http://dx.doi.org/10.17864/1947.195.

Craig, P., Ferreira, D., & Methven, J. (2017). The contrast between Atlantic and Pacific surface water fluxes. *Tellus A*, *69*(1330454).

Czaja, A. (2009). Atmospheric Control on the Thermohaline Circulation. *Journal of Climate*, *39*, 234-247.

Dai, A., & Trenberth, K. (2002). Estimates of Freshwater Discharge from Continents: Latitudinal and Seasonal Variations. *Journal of Hydrometeorology*, *3*, 660-687.

Dee, D., Uppala, S., Simmons, A., Berrisford, P., Poli, P., Kobayashi, S., ... Vitart, F. (2011). The ERA-Interim Reanalysis: configuration and performance of the data assimilation system. *Quarterly Journal of the Royal Meteorological Society*, *137*, 553-597.

Dey, D., & Döös, K. (2019). The coupled ocean–atmosphere hydrologic cycle. *Tellus A*, *71*(1650413).

Emile-Geay, J., Cane, M., Naik, N., Seager, R., Clement, A., & van Geen, A. (2003). Warren revisited: Atmospheric freshwater fluxes and "Why is no deep water formed in the North Pacific". *Journal of Geophysical Research: Oceans*, *108*. (3178)

Ferreira, D., Cessi, P., Coxall, H., de Boer, A., Dijkstra, H., Drijfhout, S., ... Wills, R. (2018). Atlantic-Pacific asymmetry in deep water formation. *Annual Reviews of Earth and Planetary Sciences*, *46*(1).

Ferreira, D., Marshall, J., & Campin, J.-M. (2010). Localization of Deep Water Formation: Role of Atmospheric Moisture Transport and Geometrical Constraints on Ocean Circulation. *Journal of*

Climate, *23*, 1456-1476.

Goswami, B., & Sengupta, D. (2003). A note on the deficiency of NCEP/NCAR reanalysis surface winds over the equatorial Indian Ocean. *Journal of Geophysical Research: Oceans*, *108*. (3124)

Leduc, G., Vidal, L., Tachikawa, K., Rostek, F., Sonzogni, C., Beaufort, L., & Bard, E. (2007). Moisture transport across Central America as a positive feedback on abrupt climatic changes. *Nature*, *445*, 908-911.

Levang, S., & Schmitt, R. (2015). Centennial Changes of the Global Water Cycle in CMIP5 Models. *Journal of Climate*, *28*, 6489-6502.

Lohmann, G. (2003). Atmospheric and oceanic freshwater transport during weak Atlantic overturning circulation. *Tellus A*, *55*, 438-449.

Manabe, S., & Stouffer, R. (1988). Two Stable Equilibria of a Coupled Ocean-Atmosphere Model. *Journal of Climate*, *1*, 841-866.

Nicholson, S. (2016). The Turkana low-level jet: mean climatology and association with regional aridity. *International Journal of Climatology*, *36*, 2598-2614.

Pfahl, S., O'Gorman, P., & Singh, M. (2015). Extratropical Cyclones in Idealized Simulations of Changed Climates. *Journal of Climate*, *28*, 9373-9392.

Richter, I., & Xie, S.-S. (2010). Moisture transport from the Atlantic to the Pacific basin and its response to North Atlantic cooling and global warming. *Climate Dynamics*, *35*, 551-566.

Riddle, E., & Cook, K. (2008). Abrupt rainfall transitions over the Greater Horn of Africa: Observations and regional model simulations. *Journal of Geophysical Research: Atmospheres*, *113*. (D15109)

Rodriguez, J., Johns, T., Thorpe, R., & Wiltshire, A. (2011). Using moisture conservation to evaluate oceanic surface freshwater fluxes in climate models. *Climate Dynamics*, *37*, 205-219.

Schiemann, R., Demory, M.-E., Mizielinski, M., Roberts, M., Shaffrey, L., Strachan, L., & Vidale, P. (2014). The sensitivity of the tropical circulation and Maritime Continent precipitation to climate model resolution. *Climate Dynamics*, *42*, 2455-2468.

Schmitt, R., Bogden, P., & Dorman, C. (1989). Evaporation Minus Precipitation and Density Fluxes for the North Atlantic. *Journal of Physical Oceanography*, *19*, 1208-1221.

Schmittner, A., Silva, T., Fraedrich, K., Kirk, E., & Lunkeit, E. (2011). Effects of Mountains and Ice Sheets on Global Ocean Circulation. *Journal of Climate*, *24*, 2814-2829.

Singh, H., Donohoe, A., Bitz, C., Nusbaumer, J., & Noone, D. (2016). Greater Moisture Transport Distances with Warming Amplify Interbasin Salinity Contrasts. *Geophysical Research Letters*, *43*, 8677-8684.

Sinha, B., Blaker, A., Hirschi, J.-M., Bonham, S., Brand, M., Josey, S., ... Marotzke, J. (2012). Mountain ranges favour vigorous Atlantic meridional overturning. *Geophysical Research Letters*, *39*. (L02705)

Steenburgh, W., Schultz, D., & Colle, B. (1998). The Structure and Evolution of Gap Outflow over the Gulf of Tehuantepec, Mexico. *Monthly Weather Review*, *126*, 2673-2691.

Stohl, A., & James, P. (2005). A Lagrangian Analysis of the Atmospheric Branch of the Global Water Cycle. Part II: Moisture Transports between Earth's Ocean Basins and River Catchments. *Journal of Hydrometeorology*, *6*, 961-984.

Trenberth, K., & Caron, J. (2001). Estimates of Meridional Atmosphere and Ocean Heat Transports. *Journal of Climate*, *14*, 3433-3443.

Trenberth, K., Fasullo, J., & Mackaro, J. (2011). Atmospheric Moisture Transports from Ocean to Land and Global Energy Flows in Reanalyses. *Journal of Climate*, *24*, 4907-4924.

Volonté, A., Turner, A., & Menon, A. (2019). Airmass analysis of the processes driving the progression of the Indian summer monsoon. *Quarterly Journal of the Royal Meteorological Society*, *in press*. doi: https://doi.org/10.1002/qj.3700

Wang, C., Zhang, L., & Lee, S.-K. (2013). Response of Freshwater Flux and Sea Surface Salinity to Variability of the Atlantic Warm Pool. *Journal of Climate*, *26*, 1249-1267.

Warren, B. (1983). Why is no deep water formed in the North Pacific? *Journal of Marine Research*, *41*, 327-347.

Wills, R., & Schneider, T. (2015). Stationary eddies and the zonal asymmetry of net precipitation and ocean freshwater forcing. *Journal of Climate*, *28*, 5115-5133.

Zaucker, F., & Broecker, W. (1992). The Influence of Atmospheric Moisture Transport on the Fresh Water Balance of the Atlantic Drainage Basin: General Circulation Model Simulations and Observations. *Journal of Geophysical Research*, *97*, 2765-2773.

Supporting Information for "Monsoon-induced zonal asymmetries in moisture transport cause anomalous Pacific precipitation minus evaporation"

P.M. Craig[1], D. Ferreira[2], and J. Methven[2]

[1]National Centre for Atmospheric Science, Department of Meteorology, University of Reading

[2]Department of Meteorology, University of Reading

Contents of this file

1. Text S1 to S4
2. Figure S1 and S2
3. Tables S1 to S3

Introduction This supplementary material contains the following material relevant to the main text:

- Text S1 describes the reanalysis dataset used in this study.
- Text S2 describes the calculations used in this study and the catchment boundaries of the ocean drainage basins.
- Text S3 compares the estimate of moisture fluxes and $\overline{P-E}$ to previous estimates.

• Figure S1 and Tables S1-S3 are not referred to in Text S1-S3 but contain information relevant to the main text. Figure S1 is referred to in Table S2.

Text S1: Data

This paper uses monthly mean vertical integrals of zonal (qu) and meridional (qv) moisture fluxes from the Interim European Centre for Medium-Range Weather Forecasts (ECMWF) Reanalysis (ERA-Interim) (Dee et al., 2011). ERA-Interim covers the period from January 1st 1979 to present; in this work we use the 36-year period spanning 1979-2014. The ECMWF forecast model (Integrated Forecasting System; IFS) has three fully coupled components for the atmosphere, land surface and ocean waves. The atmospheric component has a spectral dynamical core with a hybrid vertical η co-ordinate. The model has T255 horizontal resolution on a reduced Gaussian grid with 79 km grid spacing and 60 vertical levels. A 4D-VAR data assimilation scheme is used with 12-hourly analysis cycles which combine observations with prior information from the model. The monthly mean data we use is interpolated to a full Gaussian grid of approximately $0.7^\circ \times 0.7^\circ$ horizontal resolution.

Text S2: Methods The atmospheric moisture budget is the vertical integral of the mass continuity equation for water vapour (Berrisford et al., 2011; Craig et al., 2017):

$$\frac{\partial TCWV}{\partial t} + \frac{1}{g}\int_0^1 \nabla \cdot q\mathbf{v}\frac{\partial p}{\partial \eta}\,\mathrm{d}\eta = E - P, \tag{1}$$

where E is evaporation, P is precipitation, g is gravity, q is specific humidity, $\mathbf{v}$ is the horizontal velocity vector, p is pressure, η is the hybrid vertical co-ordinate of the ECMWF model and $TCWV = \frac{1}{g}\int_0^1 q\frac{\partial p}{\partial \eta}\,\mathrm{d}\eta$ is total column water vapour. On long time scales, the

storage term (first term on the left-hand side of equation (1)) is neglected as it is orders of magnitude (Table S1) smaller than the divergence term (second term of right-hand side) (Trenberth et al., 2011; Craig et al., 2017).

For an ocean drainage basin (the ocean and all the land which drains into it; Figure 1 in main text) the divergence term in equation (1) is linked to the vertically integrated moisture fluxes normal to the catchment boundaries through Divergence Theorem:

$$\iiint_V \nabla \cdot \mathbf{Q} \, \mathrm{d}V = \oiint_{\partial V} \mathbf{Q} \cdot \hat{\mathbf{n}} \, \frac{\partial p}{\partial \eta} \, \mathrm{d}\eta \, \mathrm{d}l, \tag{2}$$

where $\mathbf{Q} = q\mathbf{v}$, V is the volume of atmosphere above the ocean drainage basin, ∂V is the boundary of the drainage basin, $\hat{\mathbf{n}}$ is an outward-pointing unit normal vector and $\mathrm{d}l$ is the length of the boundary. Substituting equation (2) into equation (1) gives

$$\frac{1}{g} \oiint_{\partial V} \mathbf{Q} \cdot \hat{\mathbf{n}} \, \frac{\partial p}{\partial \eta} \, \mathrm{d}\eta \, \mathrm{d}l = E - P. \tag{3}$$

Note that we consider a moisture flux entering an ocean drainage basin to be positive (inward-pointing normal vector) and therefore calculate $P - E$ (positive into the surface). Throughout this paper, the vertically-integrated moisture fluxes normal to the catchment boundaries of the ocean drainage basins (Figure 1 in main paper) are calculated from monthly mean ERA-Interim (Dee et al., 2011) zonal (qu) and meridional (qv) moisture flux fields on a full Gaussian grid of approximately $0.7^\circ \times 0.7^\circ$ horizontal resolution.

The time-mean zonal and meridional moisture fluxes can be decomposed into mean flow and transient parts:

$$\overline{q\,\mathbf{v}} = \overline{q}\,\overline{\mathbf{v}} + \overline{q'\mathbf{v}'}, \tag{4}$$

where $\overline{q\,\mathbf{v}}$ is calculated from 6-hourly analysis steps, $\overline{q}\,\overline{\mathbf{v}}$ is the moisture flux explained by the time mean flow (calculated from monthly means) and $\overline{q'\mathbf{v}'}$ is the moisture flux

explained by transient processes on timescales shorter than one month. The contribution of the mean flow and transient flow to the moisture fluxes normal to the catchment boundaries and $\overline{P-E}$ can therefore be calculated from equation (4),

$$\overline{\mathbf{Q}} \cdot \hat{\mathbf{n}} \;=\; \overline{q}\,\overline{\mathbf{v}} \cdot \hat{\mathbf{n}} + \overline{q'\mathbf{v}'} \cdot \hat{\mathbf{n}}, \tag{5}$$

$$\overline{P-E} \;=\; (\overline{P-E})_{\overline{q}\,\overline{\mathbf{v}}} + (\overline{P-E})_{\overline{q'\mathbf{v}'}}. \tag{6}$$

In the main text $\overline{\mathbf{Q}} \cdot \hat{\mathbf{n}}$ is represented as Q_n, $\overline{q}\,\overline{\mathbf{v}} \cdot \hat{\mathbf{n}}$ as Q_n^m and $\overline{q'\mathbf{v}'} \cdot \hat{\mathbf{n}}$ as Q_n' (Figure S1).

The catchment boundaries of the ocean drainage basins (Figure 1 in main paper) were defined by overlaying river catchment area boundaries over orography and manually selecting points along the catchment boundary - see Craig (2019) for more details. The integrand of equation (3) is calculated at points approximately 75 km apart which is approximately the horizontal resolution of the ECMWF model (Dee et al., 2011).

Text S3: Comparing moisture fluxes and $\overline{P-E}$ to previous estimates

There are three other recent published estimates of annual mean Q_n and $\overline{P-E}$ (Rodriguez et al., 2011; Levang & Schmitt, 2015; Singh et al., 2016) calculated from ECMWF reanalysis data. Each estimate uses a different method to define the catchment boundaries of the ocean drainage basins. Compared to Figure 2 from the main text, Rodriguez et al. (2011) find a weaker Atlantic/Pacific moisture budget asymmetry of 0.3 Sv (compared to 0.47 Sv here). Singh et al. (2016) only focused on moisture fluxes in/out of the Atlantic drainage basin but their estimate of $\overline{P-E} = 0.47$ Sv matches Figure 2 from the main text. As Levang and Schmitt (2015) include the Arctic and North Atlantic in the same drainage basin it is not possible toextract a basin-scale asymmetry comparable to our

from their study.

Differences in estimates of $\overline{P-E}$ are partially due to the differing extents of the ocean drainage basins defined in each of these studies. One particularly clear issue is the catchment boundary along Central America from Singh et al. (2016) which crosses the Caribbean Sea and rejoins the continent on the eastern branch of the Andes in Colombia. This is caused by Singh et al. (2016) using the maximum topography in a longitude range to define the catchment boundaries which results in a slightly larger westward Q_n (0.46 Sv) compared to the present estimate (0.40 Sv, Figure 1 in main text).

The most notable difference in Q_n between previous studies occurs along the South-East Asian catchment boundary. The net eastward Q_n in Figure 2 from the main text (0.16 Sv) is much stronger than the eastward Q_n from Rodriguez et al. (2011) and Levang and Schmitt (2015) (0.01 Sv and 0.07 Sv respectively). This discrepancy is caused by different placements of the catchment boundary. In Rodriguez et al. (2011), the catchment boundary extends southward from the Maritime Continent before turning due east towards Australia *i.e.* the catchment boundary cuts through the open Indian Ocean. The catchment boundary from Levang and Schmitt (2015) cuts through the Maritime Continent further to the north than the present estimate's South-East Asian catchment boundary. The Levang and Schmitt (2015) catchment boundary passes through the region of moisture flux convergence which strongly affects net South-East Asian Q_n.

Further issues with South-East Asian Q_n are found in the NCEP reanalysis (Rodriguez et al., 2011) and Coupled Model Intercomparison Project Phase 5 (CMIP5) models (Levang & Schmitt, 2015). In both cases, Q_n is westward from the Pacific to the In-

dian Ocean - the opposite direction from ERA40 and ERA-Interim (Figure 1 from main text). The discrepancies between climate model and NCEP reanalysis compared to ERA-Interim may be a result of coarser resolution. For example, Schiemann et al. (2014) showed that the Walker circulation is enhanced and moisture flux convergence increases over the Maritime Continent in an atmosphere-only GCM when the resolution is increased from 350 km to 110 km. Goswami and Sengupta (2003) highlighted deficiencies in the older, low resolution NCEP reanalysis (used by Rodriguez et al. (2011)) winds over the equatorial Indian Ocean and linked these errors to deficencies in the precipitation estimate.

To test the sensitivity of the normal moisture fluxes and $P - E$ to the placement of the catchment boundaries, the moisture fluxes across approximations of the South-East Asian catchment boundary (CD in Figure 1 from the main text) from Rodriguez et al. (2011) and Levang and Schmitt (2015) (Figure S3) were calculated using ERA-Interim to compare to the flux across the boundary from Craig (2019). The equivalent integral fluxes, Q_{CD}, are 0.034 Sv and 0.099 Sv (both eastward, Indian-to-Pacific) for the Rodriguez et al. (2011) and Levang and Schmitt (2015) catchment boundaries respectively. These Q_{CD} are weaker than the 0.158 Sv from the Craig (2019) catchment boundary but are oriented in the same direction. The Rodriguez et al. (2011) Q_{CD} gives $\overline{P-E}$ of -0.51 Sv and -0.13 Sv for the Indian and Pacific Ocean drainage basins respectively, and the Levang and Schmitt (2015) Q_{CD} gives $\overline{P-E}$ of -0.58 Sv and -0.06 Sv for the Indian and Pacific basins respectively. Both these alternative calculations of Q_{CD} result in weaker net evaporation for the Indian Ocean compared to Figure 1 from the main text (-0.64 Sv) and a switch to weak net evaporation for the Pacific Ocean from the neutral moisture budget in the main

text. The normal moisture flux and $P-E$ are therefore sensitive to the placement of the catchment boundary but, in this case, not substantially enough to change the existence of $\overline{P-E}$ asymmetries (particularly when the areas of the basins are considered) or the net direction of Q_{CD}. The conclusions drawn in the main text are therefore not affected by differences in placement of catchment boundaries.

Text S4: Reasons for asymmetry in Q_n^m

Section 5.1 in the main text mentions an asymmetry in Q_n^m across 35°S. Possible reasons for the asymmetry between Atlantic, Indian and Pacific Q_n^m along 35°S (Table S2) are:

1. a greater fraction of the Atlantic is occupied by southward flux $\overline{q}\,\overline{v}$ (Figure S2) while in the Pacific the subtropical high is confined to the east of the basin (see Figure 2(b)).

2. the easterly trade winds are deflected to the south by the Andes resulting in strong southward $\overline{q}\,\overline{v}$ over South America and a region off the east coast of Brazil.

3. the South Pacific Convergence Zone may weaken $\overline{q}\,\overline{v}$ in the South Pacific as it causes anomalous moisture flux convergence into a region which has no analogue in the Atlantic (Figure S2).

References

Berrisford, P., Kållberg, P., Kobayashi, S., Dee, D., Uppala, S., Simmons, A., ... Sato, H. (2011). Atmospheric conservation properties in ERA-Interim. *Quarterly Journal of the Royal Meteorological Society*, *137*, 1381-1399.

Craig, P. (2019). *Catchment Boundaries of Ocean Drainage Basins.* University of Reading. Dataset: http://dx.doi.org/10.17864/1947.195.

Craig, P., Ferreira, D., & Methven, J. (2017). The contrast between Atlantic and Pacific surface water fluxes. *Tellus A*, *69*(1330454).

Dee, D., Uppala, S., Simmons, A., Berrisford, P., Poli, P., Kobayashi, S., ... Vitart, F. (2011). The ERA-Interim Reanalysis: configuration and performance of the data assimilation system. *Quarterly Journal of the Royal Meteorological Society*, *137*, 553-597.

Goswami, B., & Sengupta, D. (2003). A note on the deficiency of NCEP/NCAR reanalysis surface winds over the equatorial Indian Ocean. *Journal of Geophysical Research: Oceans*, *108*. (3124)

Levang, S., & Schmitt, R. (2015). Centennial Changes of the Global Water Cycle in CMIP5 Models. *Journal of Climate*, *28*, 6489-6502.

Rodriguez, J., Johns, T., Thorpe, R., & Wiltshire, A. (2011). Using moisture conservation to evaluate oceanic surface freshwater fluxes in climate models. *Climate Dynamics*, *37*, 205-219.

Schiemann, R., Demory, M.-E., Mizielinski, M., Roberts, M., Shaffrey, L., Strachan, L., & Vidale, P. (2014). The sensitivity of the tropical circulation and Maritime Continent precipitation to climate model resolution. *Climate Dynamics*, *42*, 2455-2468.

Singh, H., Donohoe, A., Bitz, C., Nusbaumer, J., & Noone, D. (2016). Greater Moisture Transport Distances with Warming Amplify Interbasin Salinity Contrasts. *Geophysical Research Letters*, *43*, 8677-8684.

Trenberth, K., Fasullo, J., & Mackaro, J. (2011). Atmospheric Moisture Transports from Ocean to Land and Global Energy Flows in Reanalyses. *Journal of Climate*, *24*,

4907-4924.

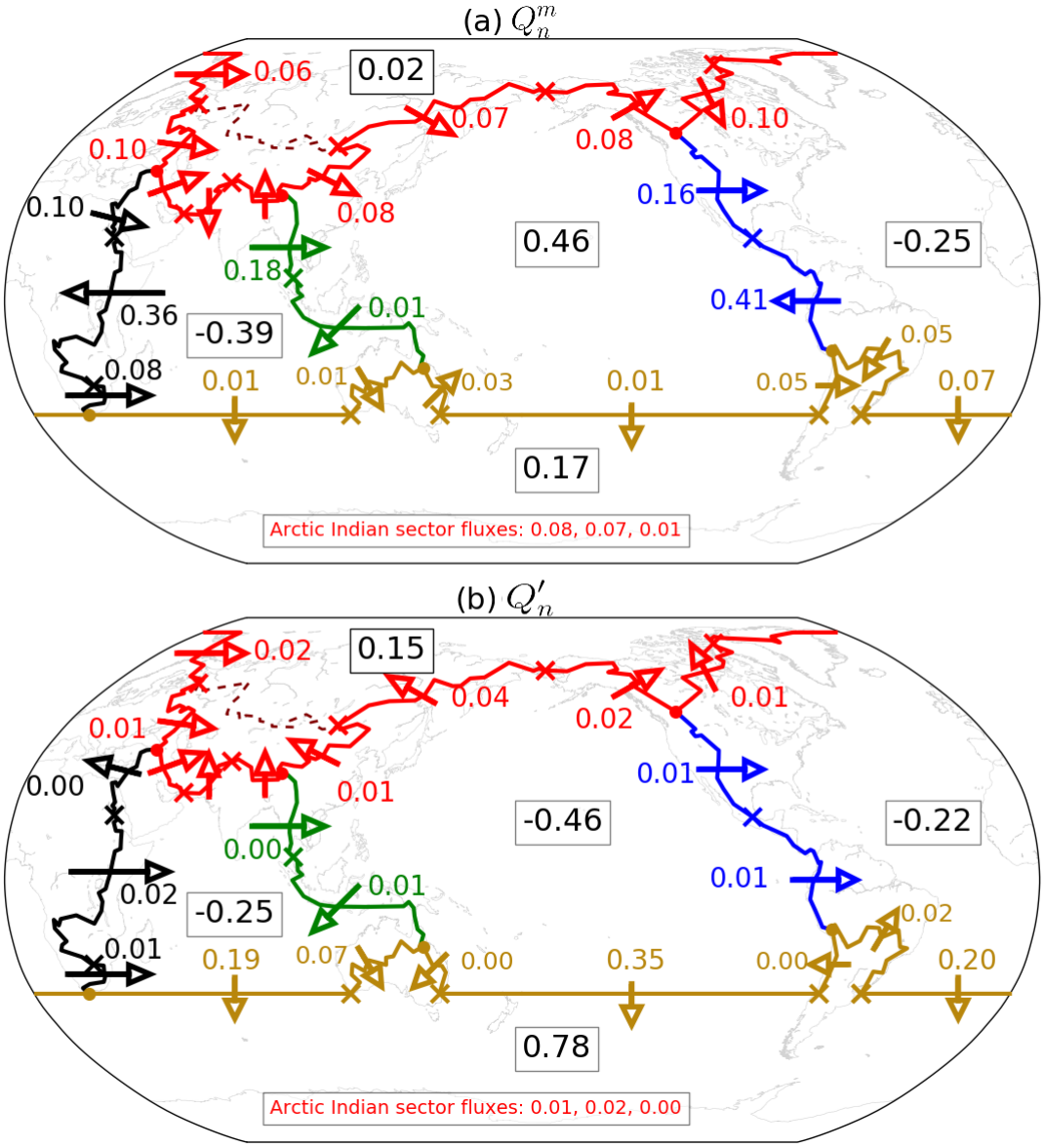

Figure S1. Reynolds decomposition of moisture fluxes normal to catchment boundaries (arrows) and $\overline{P-E}$ (boxes) into (a) monthly mean flow and (b) transient contributions. All values represent annual mean climatologies and are given in Sverdrups (1 Sv $\equiv 10^9$ kg s^{-1}).

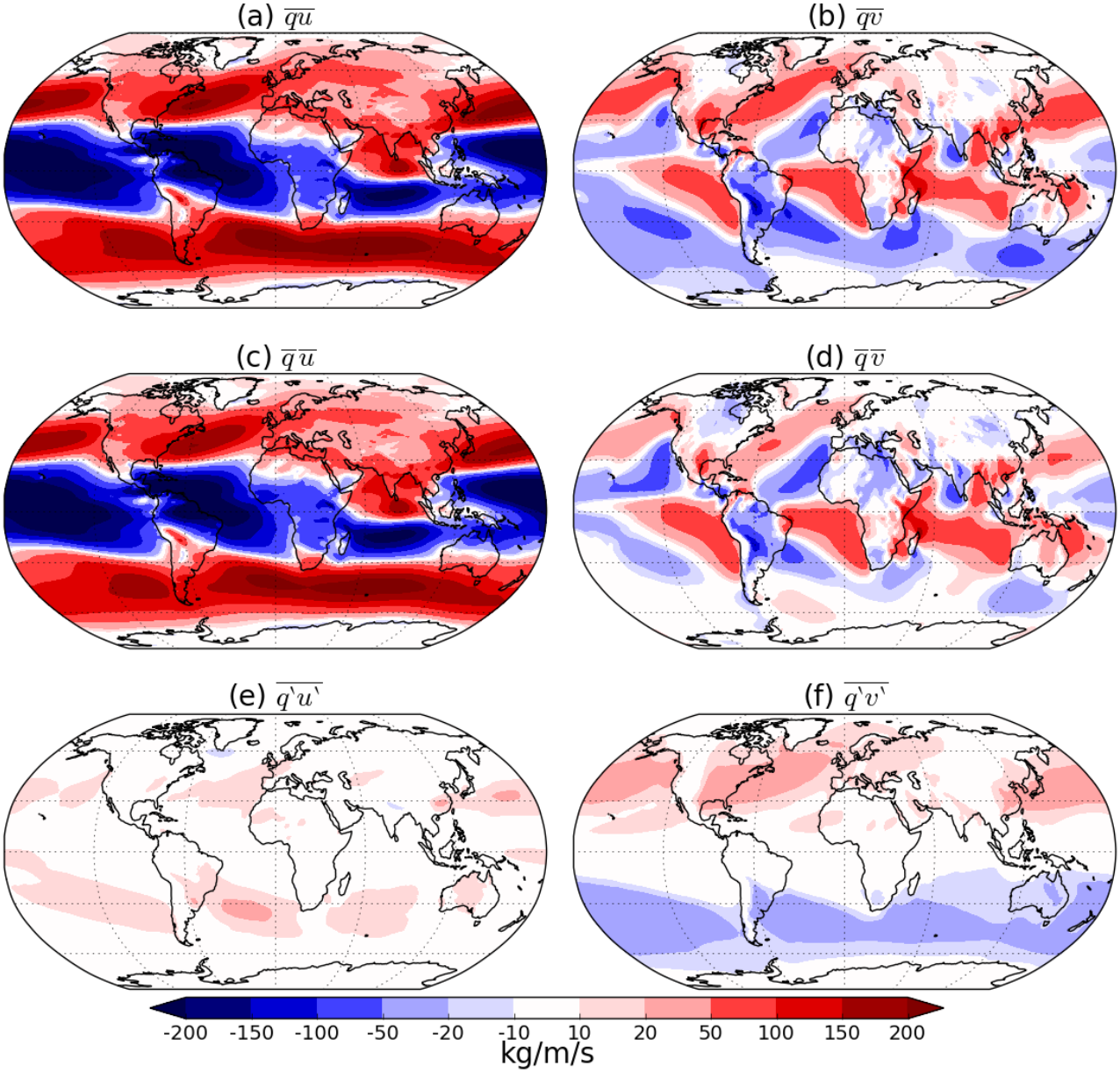

Figure S2. Reynolds decomposition of the 1979-2014 annual mean zonal (qu) and meridional (qv) moisture fluxes. Panels (a) and (b) show the annual mean climatologies for each flux; (c) and (d) show the monthly mean flow; (e) and (f) show the sub-monthly fluxes.

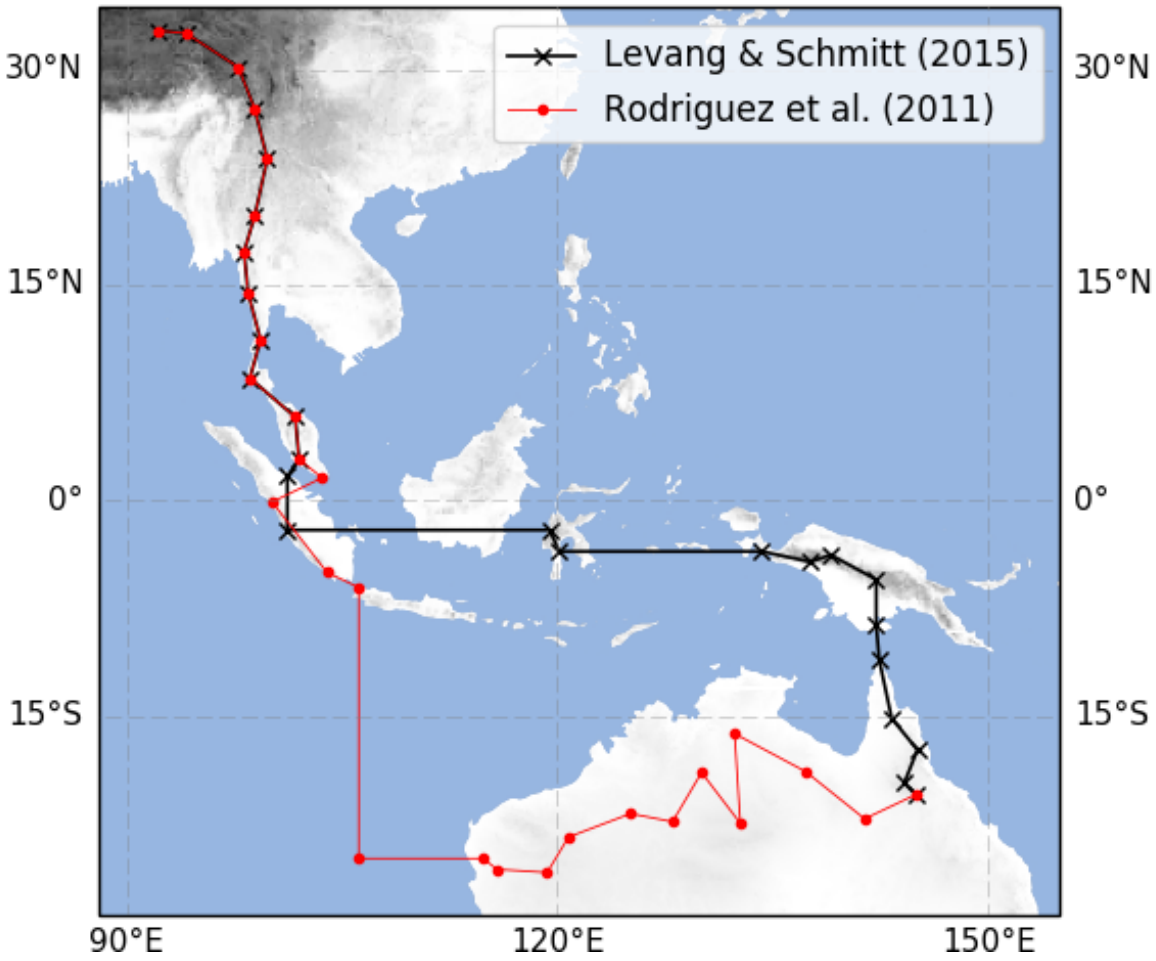

Figure S3. Approximations of the South-East Asian catchment boundaries from Levang and Schmitt (2015) in black and Rodriguez et al. (2011) in red. These catchment boundaries match the one defined by Craig (2019) until the twelfth point on the coast of Peninsular Malaysia. Between this point and the terminal point in North-East Australia the catchment boundaries approximately match those defined in the respective studies, although the final four segments of the Levang and Schmitt (2015) catchment boundary are the same as Craig (2019). The grey shading represents the Etopo05 orography.

Table S1. Climatological seasonal mean storage terms, $\partial(TCWV)/\partial t$ (see equation (1)), for each ocean drainage basin rounded to three decimal places. Units are Sverdrups.

	DJF	MAM	JJA	SON
Atlantic	0.005	-0.067	-0.032	0.084
Indian	-0.010	0.014	0.010	-0.012
Pacific	-0.008	-0.058	-0.019	0.080
Arctic	-0.002	-0.040	-0.010	0.047
Southern	-0.015	0.061	0.019	-0.051

Table S2. Net atmospheric moisture flux (Sv) and flux per unit length (10^{-8} Sv m^{-1}) across each ocean sector of 35°S. Values of Q_n are also shown in Figure 2 in the main text. Values of Q_n^m and Q_n' are shown in Figure S1.

		Q_n		Q_n^m		Q_n'	
	length (km)	Sv	10^{-8} Sv m^{-1}	Sv	10^{-8} Sv m^{-1}	Sv	10^{-8} Sv m^{-1}
Atlantic	6773.4	-0.26	-3.99	-0.07	-1.03	-0.20	-2.95
Indian	8714.4	-0.20	-2.30	-0.01	-0.12	-0.19	-2.18
Pacific	12670.4	-0.37	-2.92	-0.01	0.08	-0.35	-2.76

Table S3. Basin-integrated (Sv) and area-averaged (Sv m^{-2}) $\overline{P-E}$ for the Atlantic, Indian and Pacific Oceans from ERA-Interim (Figure 5(c) in the main text) and the idealized zonally symmetric state (Figure 5(a) in the main text). The areas (second row) are for the oceans only and do not include the land part of the drainage basins. Therefore $(\overline{P-E})_{\text{land}}$ is assumed to enter the oceans as runoff.

		Atlantic	Indian	Pacific
	Area (m^2)	0.746×10^{14}	0.450×10^{14}	1.405×10^{14}
ERA-Interim	$\overline{P-E}$ (Sv)	-0.47	-0.64	0.00
	area average (Sv/m^2)	-0.630×10^{-14}	-1.422×10^{-14}	0.00
Idealized	$\overline{P-E}$ (Sv)	-0.28	-0.18	-0.65
	area average (Sv/m^2)	-0.375×10^{-14}	-0.400×10^{-14}	-0.463×10^{-14}